Journal of Physical Science, Vol. 34(3), 1–20, 2023

The Effect of Carbonisation Heating Rates on the Properties of N-Doped Teak Sawdust Waste Activated Carbon

Dewa Ngakan Ketut Putra Negara,[1,2*] Tjokorda Gede Tirta Nindhia,[1]
Cokorda Istri Putri Kusuma Kencanawati,[1] I Gusti Agung Kade Suriadi,[3]
I Made Widiyarta,[1,2] I Putu Lokantara[1] and I Nyoman Budiarsa[1]

[1]Mechanical Engineering Department, Udayana University, Street of Bukit Jimbaran, Badung-Bali 80361, Indonesia
[2]Master Program of Mechanical Engineering, Udayana University, Jalan P.B. Sudirman, Denpasar-Bali 80234, Indonesia
[3] Industrial Engineering Department, Udayana University, Street of Bukit Jimbaran, Badung-Bali 80361, Indonesia

[*]Corresponding author: devputranegara@unud.ac.id

Published Online: 6 December 2023

To cite this article: Putra Negara, D. N. K. et al. (2023). The effect of carbonisation heating rates on the properties of N-doped teak sawdust waste activated carbon. *J. Phys. Sci.*, 34(3), 1–20. https://doi.org/10.21315/jps2023.34.3.1

To link to this article: https://doi.org/10.21315/jps2023.34.3.1

ABSTRACT: *Biomass can be utilised in place of non-renewable raw resources like coal and petroleum residue in the production of activated carbon. Each biomass, however, requires different manufacturing process parameters to obtain the desired activated carbon characteristics due to their different chemical compositions. This study aims to examine the effects of carbonisation heating rates (8°C/min, 10°C/min and 12°C/min) on the characteristics of teak sawdust-derived activated carbon. Furthermore, finding the proper carbonisation heating rate to provide the optimum characteristics is the originality of this study. Activation was carried out at a temperature of 600°C, and simultaneously, 200 mL/min of nitrogen was doped. Thermogravimetric analysis (TGA), scanning electron microscopy (SEM) and adsorption isotherm tests were performed as part of the characterisation. The results revealed that activated carbon carbonised at a rate of 10°C/min produced the best properties. This activated carbon contained 10.8% moisture, 15.26% volatile, 1.73% ash and 72.43% fixed carbon. The majority of the structure is mesopore, with an average pore diameter of 2.43 nm, a pore volume of 0.369 cm^3/g and a specific surface area of 409.698 m^2/g. Its ability to adsorb nitrogen was 239.102 cm^3/g. The successful production of activated carbon from biomass waste derived from teak sawdust offers hope for untapped sawdust waste and has the potential to be used in a number of applications that need adsorption mechanisms.*

Keywords: biomass, precursor, adsorption capacity, surface area, pore volume

1. INTRODUCTION

Biomass is a renewable raw material that can be used as a source of energy or to make other useful products. It is also known as lignocellulosic biomass due to its main chemical components being lignin, cellulose and hemicellulose.[1] Lignocellulosic biomass is a non-food, second-generation biomass feedstock that is typically composed of 35%–50% cellulose, 20%–35% hemicelluloses and 10%–25% lignin.[2] These biomass feedstocks include agricultural and forestry residues, wood and energy crops.[3] With its chemical composition and abundant quantities almost all over the world, biomass is a very promising raw material. Aside from being thermochemically convertible into biofuels,[4–7] activated carbon is another product of biomass.[8–13]

Activated carbon is a carbon-containing adsorbent with an irregular crystallographic structure formed by randomly distributed microcrystals.[14] Because of its unique pore structure with a high surface area and pore volume, activated carbon has a high porosity. The pore dimensions vary from micropores with a pore diameter of less than 2 nm, mesopores with a pore diameter of 2 nm–50 nm and macropores with a pore size of more than 50 nm [based on International Union of Pure and Applied Chemistry (IUPAC)].[15] The activated carbon pores can be cylindrical or rectangular in shape, but they can also be irregular and have a narrowing or bottleneck.[16] Because of the pore structure, activated carbon has a high adsorption ability, making it a versatile adsorbent. It has a wide range of applications, including biogas purification,[17–19] carbon dioxide (CO_2) adsorption,[20–24] methylene blue adsorption,[25–29] as a supercapacitor material,[13,30,31] as a battery material,[32,33] water treatment,[34–36] as well as others.

Activated carbon has a complex pore structure, a large specific surface area, excellent chemical stability and various oxygen-containing functional groups on the surface.[36] Because of its high degree of imperfection and the complexity of its structure, activated carbon cannot be characterised using structural formulas or chemical analysis.[16] Understanding raw materials' properties and manufacturing methods are required to produce activated carbon with superior properties for certain applications and less suitable for others.[16] Furthermore, an experiment is very useful for this purpose.

In general, the production of activated carbon involves three stages: dehydration, carbonisation and activation. Before carbonisation, the raw material is dehydrated to reduce its water content.[14] Lignocellulosic biomass is depolymerised during the carbonisation process, resulting in charcoal with a low volatile content and a high fixed carbon content. Because some of the resulting carbonisation products (mostly in the form of tar) are re-polymerised and condensed to cover the pores, the pore

structure of the charcoal produced is not perfect.[14] To increase the porosity, the tar deposits that cover these pores must be removed via an activation process that can be accomplished through physical activation, chemical activation or a combination of both. Physical activation is usually performed at higher temperatures (700°C –1000°C)[14] using activating agents like nitrogen (N_2), CO_2, argon, steam and others. Chemical activation, on the other hand, is an activation process that uses chemical activating substances such as sodium hydroxide (NaOH) and phosphoric acid (H_3PO_4). During the activation process, tar deposits are removed, basic pores formed during pyrolysis are opened, new pores are formed and existing pores are widened, resulting in activated carbon with a high level of porosity.

The formation of activated carbon microstructures, on the other hand, is highly dependent on the carbonisation and activation process conditions and parameters, such as final temperature, heating rate, holding time and gas mass flow rate.[37] Furthermore, physical parameters such as temperature, heating rate, particle size and others may influence pyrolysis end product processes.[38] The heating rate is one of the most important parameters in the biomass carbonisation process.[39] At 250ºC, it has been reported that a lower heating rate of 5ºC/min produces more carbon content (C = 53.87%) than a higher heating rate of 15ºC/min (C = 51.595%). However, at higher temperatures (450ºC and 650ºC), a higher heating rate (15ºC/min) results in a larger carbon content than a lower heating rate (5ºC/min).[40] As the carbonisation heating rate (5ºC/s–450ºC/s) increased, Kuo Zeng (2018) found that the carbon content, surface area and adsorption capability of activated carbon varied.[41] Table 1 summarises several studies on heating rate treatment, precursors used and optimal characteristics obtained.

Table 1 shows that the optimal heating rate condition is highly dependent on a variety of factors, including the type of precursor, carbonisation temperature, activating agent type and flow rate and observed response characteristics. To produce an optimal characteristic, different raw materials necessitate different heating rates. This is due to the fact that the raw materials (biomass) have distinct physical and chemical properties.

Table 1: Lists several studies on the heating rate of carbonisation.

Carbonisation parameters	Precursor	Optimum characteristic and heating rate	References
Heating rate 5ºC/min and 15ºC/min, temperature 650ºC.	Bamboo *Gigantochloa scortechinii*	C = 80.71% at 5ºC/min.	40
Heating rate 10ºC/min–30ºC/min, temperature 900ºC, holding time 3 h, N_2 flow rate 100 cm^3/min.	*Elaeis guineensis frond fiber*	SBET =555.67 m2/g, VT = 0.31 cm3/g, colour removal = 99.98%, at 10ºC/min.	42
Heating rate 0.7ºC/min, 1.0ºC/min and 1.4ºC/min. temperature 450ºC.	*Eucalyptus urograndis* and *Mimosa tenuiflora*	Yields charcoal = 36.3% (for *Eucalyptus urograndis*), = 43.3% (for Mimosa tenuiflora) at heating rate 0.7ºC /min.	39
Heating rate 10K/min–90K/min in argon flow rate of 42 ml/min, grain size of 63 > DP > 44 µm.	Mengen lignite	Yield = 57.2% at 10 K/min.	43
Heating rate 5ºC/min, 10ºC/min, 15ºC/min, N_2 flow 160 mL/min.	Pinewood	Char yield = 31.09% at 15ºC/min, 400ºC. Fix carbon = 88% at 10ºC/min, 700ºC.	44
Heating rate 5ºC/min, 10ºC/min and 20ºC/min.	Koraiensis bark	Fix carbon = 47.84%; ash = 17.85%; charcoal yield rate = 48%, 63% at 10ºC/min, 450ºC.	45
Heating rate 5ºC/s to 450ºC/s (0.083ºC/min–7.5ºC/min).	Beech wood	SBET = 140.8 m^2/g at 150ºC/s (2.5ºC/min).	41

In addition, research into the production of activated carbon has led to fresh insights into the reuse of biomaterials or throwaway items as alternative raw materials for making of activated carbon.[46] Teak sawdust waste, the biomass used in this study, is a by-product of the furniture industry, which uses teak wood (*Tectona grandis L.f.*) as its primary raw material. Some people in Bali, Indonesia, cultivate small and medium-sized industries that produce teak wood furniture, and their products are popular with both local and foreign residents. However, the teak sawdust was not being used optimally and was discarded. Converting it to activated carbon is a way to utilise and add value to this waste. There has been little research into the use of teak sawdust as a feedstock for activated carbon,[47,48] and there are still points to study about how the rate of carbonisation affects the activated carbon characteristics. In this study, the effect of carbonisation heating rates on

the physical and pore structure properties of teak sawdust-activated carbons was investigated. The heating rates used are 8ºC/min, 10ºC/min and 12ºC/min, which corresponds to a 5ºC/min–15ºC/min,[40,44] and 5ºC/min–20ºC/min range.[45] The originality of this study is in determining the ideal carbonisation heating rate to yield the optimal characteristic of activated carbon.

2. EXPERIMENTAL

2.1 Material

The source of the raw material, teak sawdust, was a small furniture factory in Klungkung-Bali, Indonesia. To get rid of contaminants, teak sawdust is cleaned with distilled water and woven through a mesh with a 60-mesh size. In order to reduce the amount of moisture in the raw material, it was then dried for three hours at 105ºC in an electric furnace. Table 2 displays the findings from an analysis of a 25 g sample utilising the Van Soest Analysis technique to determine the precursor's cellulose, hemicellulose and lignin content. In addition, a thermogravimetric analysis (TGA) test on 1 g of the precursor was carried out; the outcomes are displayed in Table 3.

Table 2: Van Soest analysis of precursor.

Chemical composition of precursor/ teak sawdust (%)		
Cellulose	Hemicellulose	Lignin
43.72	11.38	31.26

3. PREPARATION OF ACTIVATED CARBON

Figure 1 depicts the placement of a carbonisation reactor in a controlled electric furnace with 25 g of hydrated teak sawdust. With a heating rate of 8ºC/min, the sample was heated to a temperature of 600ºC and immediately activated by continuously flowing N_2 at a rate of 200 mL/min for 100 min, controlled by a flowmeter. Furthermore, the sample was cooled in the furnace until it reached room temperature while still being fed N_2 for 30 min. Activated carbon samples were collected from the activation reactor and stored in an airtight container. The same procedures were followed for carbonisation heating rates of 10ºC/min and 12ºC/min. The resulting activated carbons were designated as AC-CR8, AC-CR10 and AC-CR10 for activated carbon carbonised at 8ºC/min, 10ºC/min and 12ºC/min, respectively, as shown in Figure 2b.

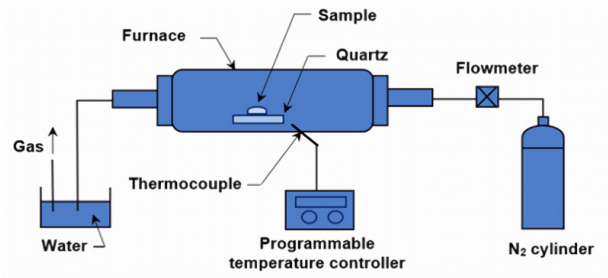

Figure 1: Experimental set up in producing of activated carbon.

3.1 Characterisation of Activated Carbons

Activated carbons are characterised using TGA, scanning electron microscope (SEM) and adsorption isotherm testing. A TGA 701, ASTM D7582 MVA in coal, 0.02% relative standard deviation (RSD) precision device is used to determine the ash, volatile, fixed carbon and moisture of the precursor and activated carbons. Using a SEM-JSM-651OLA instrument, the surface morphology of activated carbons was examined. Utilising Quantachrome Instruments version 10.01, the adsorption isotherm test was conducted after outgassing the material for three hours at 300°C. N_2 was the gas under investigation; the analysis took 175.1 min, and the bath temperature was 77.35K. This test measures the pore surface area (S_{BET}), pore volume (V_P), pore diameter (D_P), pore size distribution (P_{SD}) and N_2 adsorption capability of activated carbon.

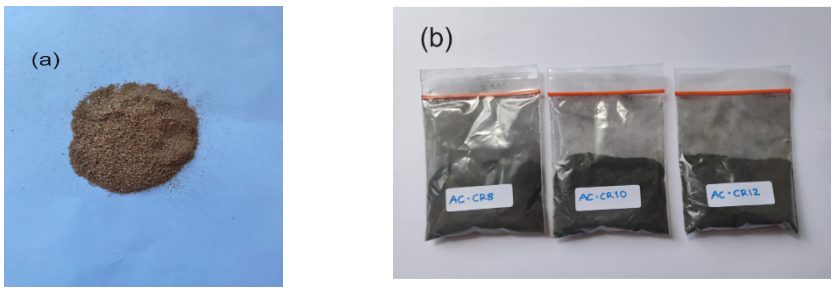

Figure 2: (a) Teak sawdust; (b) Activated carbons produced.

4. RESULTS AND DISCUSSION

4.1 TGA Analysis of Precursor

TGA is a widely used method for precisely measuring the weight loss of a small volume of sample when subjected to controlled temperature profiles and heating rates.[5] It is primarily graphical representations of sample mass versus time or temperature.[49] At certain temperatures, the material will lose a significant amount of mass when heated continuously from room temperature. Mass loss at a specific temperature can indicate test material content and is highly dependent on the chemical composition of the raw materials, particularly lignin, cellulose and hemicellulose. Since the lignin, cellulose and hemicellulose content of each raw material varies, so do the temperatures and times needed for decomposition. Teak sawdust consists of 43.72% cellulose, 11.38% hemicellulose and 31.26% lignin as shown in Table 2. Decomposition of hemicellulose took place at temperatures ranging from 223.4ºC–332.8ºC, cellulose at 326.8ºC–369.7ºC and lignin at 311.5ºC–461.3ºC.[50] Other researchers reported that thermal degradation of cellulose, hemicellulose and lignin occurs at 300ºC–400ºC,[51] 200ºC–350ºC[52] and 600ºC–700ºC,[53] respectively.

Figure 3 shows that the decomposition of the precursor begins with a mass loss of about 11% between the 25th and 45th min at temperatures ranging from 30ºC–110ºC . The evaporation of a small amount of water vapour in the precursor causes this mass loss. The weight loss remained constant at 11% from 46th to 135th min, up to a temperature of 270ºC. The precursor drying process takes the form of a decrease in water content during this time. After the precursor dries, the temperature rises to 330ºC, with a 30% weight loss and the mass loss reaches 38% up to a temperature of 390ºC. At a temperature of 270ºC–390ºC, it takes approximately 95 min to lose 38% mass. Hemicellulose and some lignin decompose at temperatures ranging from 270ºC–330ºC,[50–52] while cellulose and more lignin decompose at temperatures ranging from 330ºC–390ºC.[49] Further lignin decomposition occurs at temperatures ranging from 390ºC–950ºC,[50] with up to 80% mass loss. In addition, the ashing process is carried out, in which the temperature is reduced to 600ºC while oxygen is pumped into the reactor to start the combustion process. When the temperature reaches 750ºC, the mass reduction percentage reaches 98.16%, with the remainder being ash (1.84%).

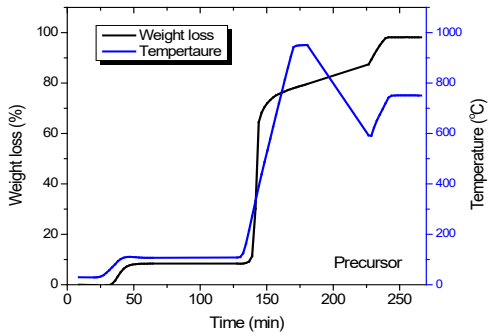

Figure 3: The relationship between weight loss, time and temperature of precursor.

The values of the precursor proximate analysis are shown in Table 3. The precursor's moisture, volatile, ash and fixed carbon content are 8.37%, 71.23%, 1.84% and 18.56%, respectively. The moisture content of various biomass (Siam weed, Gmeliana arborea, sugarcane straw, rice husk, shea butter wood, palm kernel shell, bamboo wood) has been reported to range from 0.18% to 2.19% which is lower than the moisture of the precursor.[54] The other proximate elements of the precursor are in the range of those biomass's volatiles, ash and fixed carbon, with 61.80%–85.20%, 0.94%–20.89% and 11.14%–22.40%, respectively.[54] Felix (2022), reported that the teak sawdust's moisture, volatile, ash and fixed carbon are 3.87%, 78.17%, 3.53% and 14.43%, respectively.[49] Ramires (2020) discovered that the TGA teakwood sawdust elements were 5.05% moisture, 83.92% volatile matter, 15.67% fixed carbon and 0.41% ash.[48] The difference in the proximate element percentage of the precursors used in this study was caused by several factors, including age, where the plant grew, habitat (place of life), climate, nutrient availability and others.

Table 3: TGA analysis of precursor and activated carbons produced.

Samples	The values of TGA elements (%)			
	Moisture	Volatile	Ash	Fix carbon
Precursor	8.37	71.23	1.84	18.56
AC-CR8	9.15	11.55	5.26	74.04
AC-CR10	10.58	15.26	1.73	72.43
AC-CR12	8.93	11.30	5.89	73.88

4.2 The Effect of Heating Rate on the TGA Elements of Activated Carbons

The three activated carbons exhibit the same pattern in terms of thermal stability and thermogravimetric behaviour, but they require different amounts of time and temperature to attain mass reduction stability, as seen in Figure 4(a), (b) and (c). For the precursor and the three activated carbons, Figure 5(a) and (b) illustrate the link between mass loss and temperature as well as the association between mass loss and time.

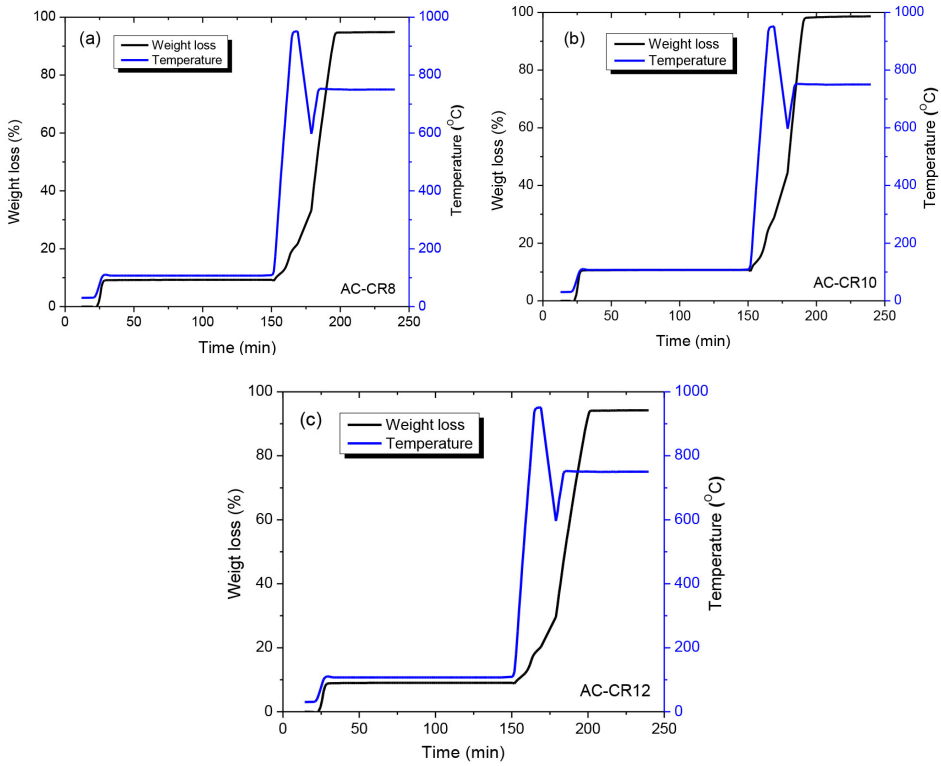

Figure 4: The relationship between weight loss, time and temperature of samples (a) AC-CR8, (b) AC-CR10 and (c) AC-CR12.

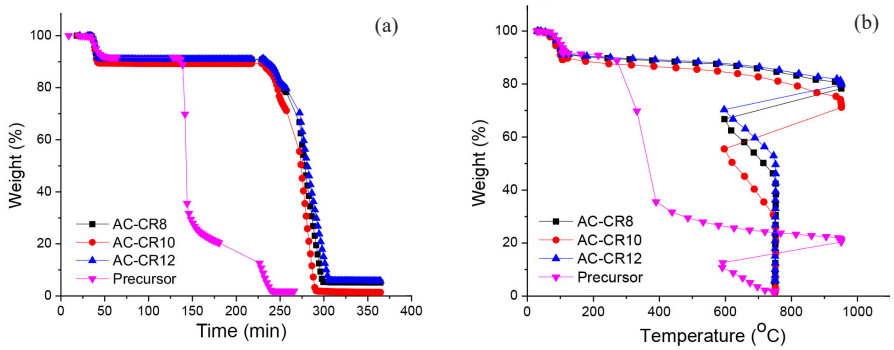

Figure 5: (a) The weight loss and time relationship of the precursor and activated carbons, (b) The weight loss and temperature relationship of precursor and activated carbons.

It can be seen that the activation rate has a varying effect on mass changes. Heating from room temperature to 107ºC is a moist process, meaning it reduces the water content of the specimen.[29] Until a temperature of 107ºC, the remaining mass of AC-CR8 is approximately 90.75%, while the mass of AC-CR10 and AC-CR12 is approximately 91.0% and 89.250%, respectively. In other words, the initial mass losses for AC-CR8, AC-CR10 and AC-CR12 were 9.25%, 9% and 10.75%, respectively. This process lasts approximately 180 min at a constant temperature of 107ºC. The percentage of mass reduction is proportional to the moisture content of the sample (AC-CR10 > AC-CR8 > AC-CR12), with the higher the moisture content, the greater the mass reduction. The temperature range of initial mass loss of activated carbon from different precursor is also different. Mohd Azani et al., reported that the initial mass loss activated carbon derived from rubber seed shell occurred in the range of 29ºC–144ºC with a percentage loss of 4.59%.[29]

Furthermore, due to the reduced volatile content, mass loss occurs rapidly as the temperature rises to 951.5ºC. Samples with the highest volatile content also experienced the greatest mass reduction. The remaining mass of the sample at 951.5ºC was 79.6%, 78% and 70.9% for AC-CR8, AC-CR10 and AC-CR12, respectively. Furthermore, the test temperature is reduced to 600ºC while oxygen begins to flow, allowing the combustion process to continue until ash is formed. Along with continued heating, there was another decrease in sample mass due to the reduction of other gases during the combustion process until the formation of ash at 750ºC. The ash mass was the remaining mass at the end of the test, which was 5.26%, 1.73% and 5.89% for AC-CR8, AC-CR10 and AC-CR12, respectively.

The effect of the carbonisation heating rate on the resulting proximate component varied as well. By increasing the carbonisation heating rate from 8ºC/min to 10ºC/min, the moisture and volatile values increased while the fixed carbon and ash values decreased. When the carbonisation rate was raised from 10ºC/min to 12ºC/min, the moisture and volatiles decreased while the fixed carbon and ash increased, as shown in Table 3.

4.3 The Effect of Heating Rate on the Pore Structure of Activated Carbons

The pore structure parameters of the activated carbons, such as specific S_{BET}, P_{SD} and V_P, were determined by the N_2 adsorption isotherm test.[55] Figure 6 depicts the graph of the N_2 adsorption isotherm, while Figure 7 depicts the P_{SD}. The heating rate of carbonisation also has a fluctuating effect on the pore structure of the activated carbon. An increase in the heating rate from 8ºC/min–10ºC/min causes a significant increase in N_2 uptake. However, from the carbonisation heating rate of 10ºC/min–12ºC/min, the increase in relative pressure has no significant effect on increasing N_2 adsorption. At each level of relative pressure, the amount of N_2 adsorbed in AC-CR12 is much smaller than that of AC-CR10. The order of level N_2 adsorption at each relative pressure change is AC-CR10 > AC-CR8 > AC-CR12.

The N_2 adsorption capacity increased proportionally until reaching a relative pressure of 1 for AC-CR10, while for AC-CR 8 and AC-AR12, the increase in N_2 adsorption capacity was not significant. The absence of significant N_2 uptake at relative pressures below 0.05 indicates that the three activated carbons are mainly mesopores, supplemented by a small number of micropores.[55]

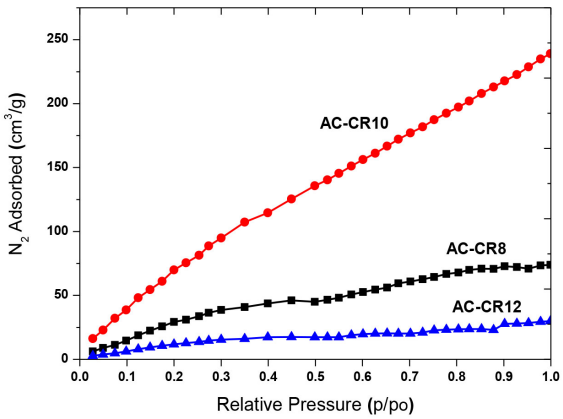

Figure 6: Adsorption isotherm of activated carbons.

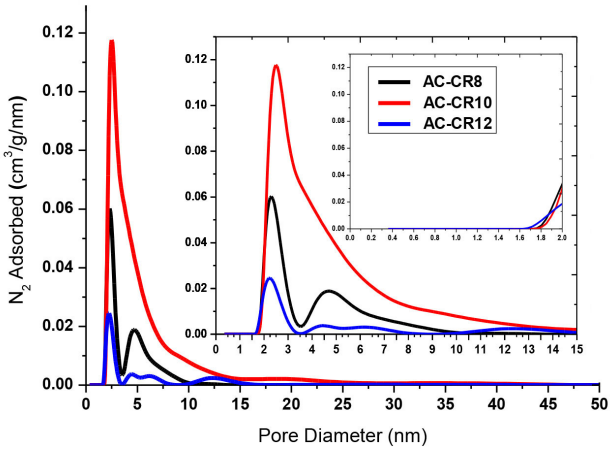

Figure 7: P_{SD} of activated carbons.

The carbonisation heating rates affects the different P_{SD} of activated carbons, as shown in Figure 7. The P_{SD} of AC-CR8 was mainly distributed at 1.7 nm–12 nm with two peaks (bimodal distribution); the P_{SD} of AC-CR10 was spread at 1.7 nm–44 nm with one peak (monomodal distribution); while the P_{SD} of AC-CR12 was distributed at 1.7 nm–17.5 nm with four peaks (multimodal distribution). The three activated carbons have a pore structure, as seen in Figure 7, with the majority of the mesopores being between 2 nm and 50 nm in size and the minority being smaller than 2 nm in size. This is corroborated by Table 4's display of the average D_P of the three activated carbons in the mesopore.

The S_{BET} of AC-CR8, AC-CR10 and AC-CR12 activated carbons were 180.285 m^2/g, 409.698 m^2/g and 67.839 m^2/g, respectively, with total V_P of 0.109 cm^3/g, 0.369 cm^3/g and 0.043 cm^3/g and average D_P of 2.43 nm, 3.61 nm and 2.54 nm. This also demonstrates that the carbonisation heating rate has a fluctuating effect on the S_{BET}, total V_P and average D_P. The order of S_{BET} and total V_P is AC-CR10 > AC-CR8 > AC-CR12, while the D_P is AC-CR10 > AC-CR12 > AC-CR8. This also has implications for the amount of N_2 that can be absorbed at a relative pressure of 1, where activated carbon which has the highest S_{BET} and V_P has the highest N_2 adsorption as well, as shown in Figure 8. The order of adsorption of activated carbon to N_2 is AC-CR10. >AC-CR8>AC-CR12, in line with the order of S_{BET} and total V_P.

Table 4: Surface structural of activated carbons.

Samples	S_{BET} (m^2/g)	V_P (cm^3/g)	D_P (nm)
AC-CR8	180.285	0.109	2.43
AC-CR10	409.698	0.369	3.61
AC-CR12	67.839	0.043	2.54

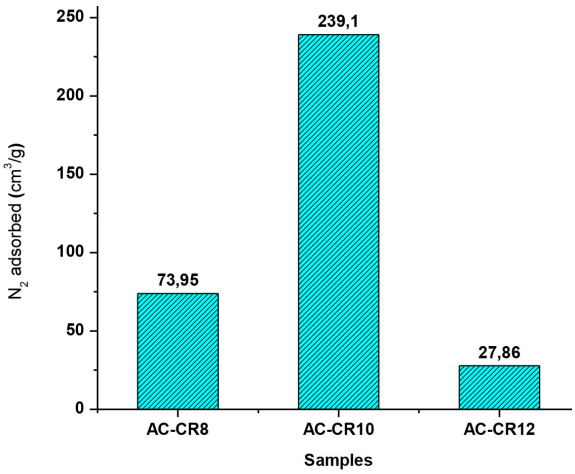

Figure 8: N_2 adsorption capacity of activated carbons.

The heating rate determines the gas formation and diffusion rates, which control the formation of the pore structure during carbonisation.[56] Pore structures vary depending on the heating rate. The best heating rate can only be determined by experimentation; it cannot be anticipated. The specific S_{BET}, V_P and P_{SD} of activated carbon as well as the kind of substance adsorbed (adsorbate) have a significant impact on its ability to adsorb substances.[57] Higher V_P and S_{BET} activated carbon typically has superior adsorption capacity. Activated carbon with a higher V_P and S_{BET} generally has a better adsorption capacity. Additionally, the adsorption capacity of activated carbon is also significantly influenced by the P_{SD}.[57,58] With the same P_{SD}, activated carbon may have varying adsorption capacities for various substances. On the other hand, when used to adsorb the same adsorbate, activated carbon with different pore size distributions may have varying adsorption capabilities. Adsorbate has unique characteristics based on the size of its molecules. Only substances whose molecular diameter is equal to or lower than the activated carbon's D_P can be absorbed.

4.4 Surface Morphology of Activated Carbons

Figures 9, 10 and 11 for AC-CR8, AC-CR10 and AC-CR12, respectively, show the pictures that were produced after SEM was used to observe the surface morphology of the activated carbon. The resulting surface morphology consists of carbon nano-thin sheets that form grooves. The grooves of AC-CR12 are mostly covered by debris, ash or collapse of the carbon atom skeletons. This is consistent with the fact that AC-CR12 has the highest ash content, the lowest surface area, pore-volume and N_2 adsorption capacity compared to AC-CR8 and AC-CR10. The shape of the pore grooves varies, most of them are elongated with diameters mostly resembling circles and irregular shapes. Based on the resulting SEM image, the order of the number of pores produced is AC-CR10 > AC-CR8 > AC-CR12. In general, this study found that the optimal heating rate of carbonisation is 10ºC/min because it produces the highest S_{BET}, V_P, N_2 adsorption capacity and lowest ash content. The same optimum carbonisation heating rate of 10ºC/min were in accordance with some studies[41–44] although the raw materials used and the characteristics observed were different.

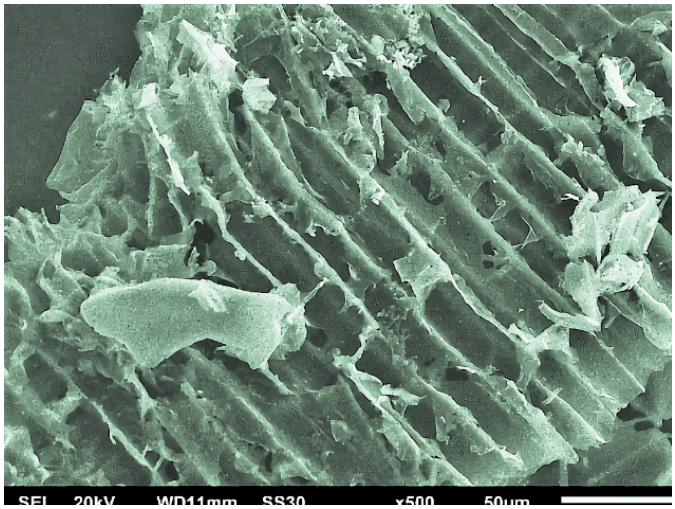

Figure 9: SEM image of AC-CR8.

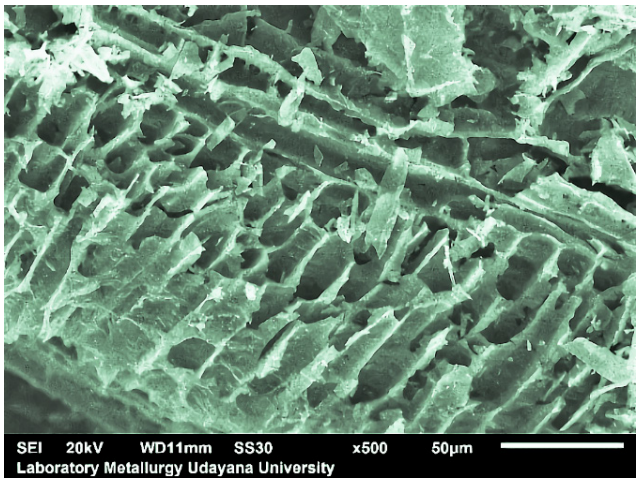

Figure 10: SEM image of AC-CR10.

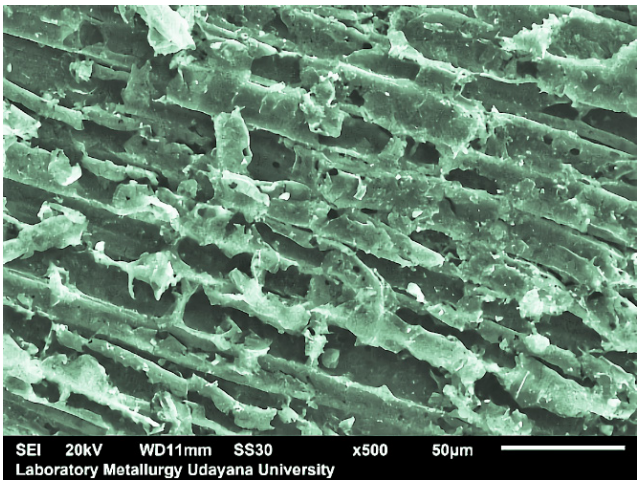

Figure 11: SEM image of AC-CR12.

5. CONCLUSIONS

Various carbonisation heating rates were used to successfully convert waste teak sawdust into activated carbon, which produced various properties. The carbonisation heating rate has a fluctuating effect on the composition of the proximate and the pore structure of the activated carbons. The ranges for the activated carbons' moisture, volatiles, ash and fixed carbon were 8.93%–10.58%, 11.3%–

15.26%, 1.73%–5.89% and 72.43%–74.04%, respectively. In the meantime, the measured S_{BET}, total V_P and average D_P all ranged from 67.839 m^2/g–40.698 m^2/g, 0.043 cm^3/g–0.369 cm^3/g and 2.43 nm–3.61 nm, respectively. The greatest outcomes are obtained with activated carbon carbonised at a heating rate of 10ºC/min (AC-CR10). This activated carbon has the largest S_{BET} surface area and V_P (409.698 m^2/g and 0.369 cm^3/g), the D_P of 3.61 nm, the lowest ash content (1.73%) and the highest N_2 adsorption capacity (239.102 cm^3/g). In addition to successfully turning teak sawdust waste into activated carbon, this product (AC-CR10) also has the potential to be employed in a number of other applications, including the purification of biogas, the adsorption of CO_2 and methylene blue, among others. The shortcoming of this study is that it only looks at the effects of heating rate carbonisation on pore structure, TGA elements and activated carbon morphology without considering how it relates to changes in crystal structure, interactions with surface morphology and gas adsorption mechanisms, all of which need to be thoroughly studied in the future.

6. ACKNOWLEDGEMENTS

We sincerely appreciate the support granted for this work by the Research and Community Service of Udayana University (LPPM Unud) under the Udayana Superior Research (PUU) scheme for the 2021 budget year under contract number B/96-206/UN14.4.A/PT.01.05/2021.

REFERENCES

1. Bahri, S. et al. (2021). Rational design of process parameters for carbon-neutral and sulfur-free motor fuel production from second-generation biomass generated syngas. *J. Clean. Prod.*, 279, 123559. https://doi.org/10.1016/j.jclepro.2020.123559
2. Ma, J. et al. (2019). Advances in catalytic conversion of lignocellulose to chemicals and liquid fuels. *J. Energy Chem.*, 36, 74–86. https://doi.org/10.1016/j.jechem.2019.04.026
3. Di Blasi, C. (2009). Combustion and gasification rates of lignocellulosic chars. *Prog. Energy Combust. Sci.*, 35(2), 121–140. https://doi.org/10.1016/j.pecs.2008.08.001
4. Elgarahy, A. M. et al. (2021). Thermochemical conversion strategies of biomass to biofuels, techno-economic and bibliometric analysis: A conceptual review. *J. Environ. Chem. Eng.*, 9(6), 106503. https://doi:10.1016/j.jece.2021.106503
5. Ong, H. C. et al. (2020). A state-of-the-art review on thermochemical conversion of biomass for biofuel production: A TG-FTIR approach. *Energy Convers. Manag.*, 209, 112634. https://doi.org/10.1016/j.enconman.2020.112634

6. Rocha, D. N. et al. (2020). Improving biofuel production by thermochemical conversion of defatted Scenedesmus obliquus biomass. *J. Clean. Prod*., 275. https://doi.org/10.1016/j.jclepro.2020.124090
7. Aliyu, A. et al. (2021). Microalgae for biofuels: A review of thermochemical conversion processes and associated opportunities and challenges. *Bioresour. Technol. Reports*, 15, 100694. https://doi.org/10.1016/j.biteb.2021.100694
8. Putra Negara, D. N. K. et al. (2020). Textural characteristics of activated carbons derived from tabah bamboo manufactured by using H_3PO_4 chemical activation. *Mater. Today Proc*., 22, 148–155. https://doi.org/10.1016/j.matpr.2019.08.030
9. Serafin, J. et al. (2017). Highly microporous activated carbons from biomass for CO_2 capture and effective micropores at different conditions. *J. CO2 Util*., 18, 73–79. 2017, https://doi.org/10.1016/j.jcou.2017.01.006
10. Nowrouzi, M. et al. (2018). Superior CO_2 capture performance on biomass-derived carbon/metal oxides nanocomposites from Persian ironwood by H_3PO_4 activation. *Fuel*, 223, 99–114. https://doi.org/10.1016/j.fuel.2018.03.035
11. Putra Negara, D. N. K. et al. (2020). Development and characterization of activated carbons derived from lignocellulosic material. *Mater. Sci. Forum*, 988, 80–86. https://doi.org/10.4028/www.scientific.net/MSF.988.80
12. Tyagi, U. et al. (2019). Simultaneous pretreatment and hydrolysis of hardwood biomass species catalyzed by combination of modified activated carbon and ionic liquid in biphasic system. *Bioresour. Technol*., 289, 121675. https://doi.org/10.1016/j.biortech.2019.121675
13. Taer, E. et al. (2020). Conversion Syzygium oleana leaves biomass waste to porous activated carbon nanosheet for boosting supercapacitor performances. *J. Mater. Res. Technol*., 9 (6), 13332–13340. https://doi.org/10.1016/j.jmrt.2020.09.049
14. Pallarés J. et al. (2018). Production and characterization of activated carbon from barley straw by physical activation with carbon dioxide and steam. *Biomass and Bioenergy*, 115, 64–73. https://doi.org/10.1016/j.biombioe.2018.04.015
15. Thommes, M. et al. (2015). Physisorption of gases, with special reference to the evaluation of surface area and pore size distribution (IUPAC Technical Report). *Pure Appl. Chem*., 87, 1051–1069. https://doi.org/10.1515/pac-2014-1117
16. McDougall, G. J. (1991). Physical nature and manufacture of activated carbon. *J. South African Inst. Min. Metall*., 91(4), 109–120. https://api.semanticscholar.org/CorpusID:53551280
17. Farooq, M. et al. (2017). Bio-methane from an-aerobic digestion using activated carbon adsorption. *Anaerobe*, 46, 33–40. https://doi.org/10.1016/j.anaerobe.2017.05.003
18. Gil, M. V. et al. (2015). Carbon adsorbents for CO_2 capture from bio-hydrogen and biogas streams: Breakthrough adsorption study. *Chem. Eng. J.*, 269, 148–158. https://doi.org/10.1016/j.cej.2015.01.100
19. Angelidaki, I. et al. (2018). Biogas upgrading and utilization: Current status and perspectives. *Biotechnol. Adv*., 36(2), 452–466. https://doi.org/10.1016/j.biotechadv.2018.01.011

20. Akkarawatkhoosith, N. et al. (2019). High-throughput CO_2 capture for biogas purification using monoethanolamine in a microtube contactor. *J. Taiwan Inst. Chem. Eng*., 98, 113–123. https://doi.org/10.1016/j.jtice.2018.05.002
21. Ahmed, M. B. et al. (2019). Activated carbon preparation from biomass feedstock: Clean production and carbon dioxide adsorption. *J. Clean. Prod.*, 225, 405–413. https://doi.org/10.1016/j.jclepro.2019.03.342
22. Gong, H. et al. (2019). Effect of volatile organic compounds on carbon dioxide adsorption performance via pressure swing adsorption for landfill gas upgrading. *Renew. Energy*, 135, 811–818. https://doi.org/10.1016/j.renene.2018.12.068
23. Ferella, F. et al. (2017). Separation of carbon dioxide for biogas upgrading to biomethane. *J. Clean. Prod*., 164, 1205–1218. https://doi.org/10.1016/j.jclepro.2017.07.037
24. Han, J. et al. (2018). The N-doped activated carbon derived from sugarcane bagasse for CO_2 adsorption. *Ind. Crops Prod*., 128, 290–297. https://doi.org/10.1016/j.indcrop.2018.11.028
25. Kuang, Y. et al. (2020). Adsorption of methylene blue in water onto activated carbon by surfactant modification. *Water*, 12, 1–19. https://doi.org/10.3390/w12020587
26. Jawad, A. H. et al. (2016). Adsorption of methylene blue onto activated carbon developed from biomass waste by H_2SO_4 activation: Kinetic, equilibrium and thermodynamic studies. *Desalin. Water Treat*., 57(52), 25194–25206. https://doi.org/10.1080/19443994.2016.1144534
27. Ben Nasr, J. et al. (2017). Characterization of activated carbon prepared from sludge paper for methylene blue adsorption. *J. Mater. Environ. Sci*., 8(6), 1960–1967.
28. Nuhu, A. A. et al. (2019). Equilibrium adsorption studies of methylene blue onto caesalpinia pulcherrima husk-based activated carbon. *Chem. Sci. Int. J*., 2(5), 1–11. https://doi.org/10.9734/csji/2019/v26i330096
29. Mohd. Azani, N. F. S. et al. (2019). Characterisation and kinetic studies on activated carbon derived from rubber seed shell for the removal of methylene blue in aqueous solutions. *J. Phys. Sci.*, 30(2), 1–20. https://doi.org/10.21315/jps2019.30.2.1
30. Dos Reis, G. S. et al. (2021). Flexible supercapacitors of biomass-based activated carbon-polypyrrole on eggshell membranes. *J. Environ. Chem. Eng*., 9(5). https://doi.org/10.1016/j.jece.2021.106155
31. Zhang, X. et al. (2021). High-performance discarded separator-based activated carbon for the application of supercapacitors. *J. Energy Storage*, 44, 103378. https://doi.org/10.1016/j.est.2021.103378
32. Nguyen, D. T. et al. (2020). A water-activated paper-based battery based on activated carbon powder anode and $CuCl_2$/CNT cathode. *Energy Reports*, 6, 215–219. https://doi.org/10.1016/j.egyr.2020.11.259
33. Li, S. et al. (2020). Cellulose substance derived nanofibrous activated carbon as a sulfur host for lithium-sulfur batteries. *Colloids Surfaces A Physicochem. Eng. Asp*., 602, 125129. https://doi.org/10.1016/j.colsurfa.2023.131331

34. Nakazawa, Y. et al. (2021). Differences in removal rates of virgin/decayed microplastics, viruses, activated carbon, and kaolin/montmorillonite clay particles by coagulation, flocculation, sedimentation, and rapid sand filtration during water treatment. *Water Res.*, 203, 117550. https://doi.org/10.1016/j.watres.2021.117550
35. Oladimeji, T. E. et al. (2021). Production of activated carbon from sawdust and its efficiency in the treatment of sewage water. *Heliyon*, 7(1), e05960. https://doi.org/10.1016/j.heliyon.2021.e05960
36. Sera, P. R. et al. (2021). Potential of valourized moringa oleifera seed waste modified with activated carbon for toxic metals decontamination in conventional water treatment. *Bioresour. Technol. Reports*, 16, 100881. https://doi.org/10.1016/j.biteb.2021.100881
37. Patil, B. S. & Kulkarni, K. S. (2012). Development of high surface area activated carbon from waste material. *Int. J. Adv. Eng. Res. Stud*., I(II), 2249–8974.
38. Oyedun, A. O. et al. (2012). Kinetic modelling and analysis of waste bamboo pyrolysis. *Chem. Eng. Trans*., 29, 697–702. https://doi.org/10.3303/CET1229117
39. César, L. et al. (2019). Effect of pyrolysis heating rate on the chemical composition of wood vinegar from eucalyptus urograndis and mimosa tenuiflora. *Rev. Árvore*, 43(4), 1–11. https://doi.org/10.1590/1806-90882019000400008
40. Munirah, N. R. et al. (2015). Characteristics of carbonized bamboo at various temperatures. *Appl. Mech. Mater*., 754–755, 115–119. https://doi.org/10.4028/www.scientific.net/AMM.754-755.115
41. Zeng, K. et al. (2015). The effect of temperature and heating rate on char properties obtained from solar pyrolysis of beech wood. *Bioresour. Technol*., 182, 114–119. https://doi.org/10.1016/j.biortech.2015.01.112
42. Low, L. W. et al. (2015). Carbonization of Elaeis guineensis frond fiber: Effect of heating rate and nitrogen gas flow rate for adsorbent properties enhancement. *J. Ind. Eng. Chem*., 28, 37–44. https://doi.org/10.1016/j.jiec.2015.01.020
43. Güldoğan, Y. et al. (2001). Effects of heating rate and particle size on pyrolysis kinetics of mengen lignite. *Energy Sources*, 23(4), 337–344. https://doi.org/10.1080/009083101300110887
44. Li, A. et al. (2016). Effects of temperature and heating rate on the characteristics of molded bio-Char. *BioResources*, 11(2), 3259–3274. https://doi.org/10.15376/biores.11.2.3259-3274
45. Huang, H. et al. (2015). Experimental study on impact of heating temperature and heating rate during carbonization of woody biomass. Proceedings of the 2nd International Conference on Green Materials and Environmental Engineering. *Adv. Eng. Res.*, 174–178. https://doi.org/10.2991/gmee-15.2015.46
46. Ghani, N. I. A. et al. (2017). Modification of activated carbon from biomass nypa and amine functional groups as carbon dioxide adsorbent. *J. Phys. Sci.*, 28(1), 227–240. https://doi.org/10.21315/jps2017.28.s1.15
47. Kumar, A. & Gupta, H. (2020). Activated carbon from sawdust for naphthalene removal from contaminated water. *Environ. Technol. Innov*., 20, 101080. https://doi.org/10.1016/j.eti.2020.101080

48. Ramirez, A. et al. (2020). Removal of Cr (VI) from an aqueous solution using an activated carbon obtained from teakwood sawdust: Kinetics, equilibrium, and density functional theory calculations. *J. Environ. Chem. Eng.*, 8(2), 103702. https://doi.org/10.1016/j.jece.2020.103702
49. Felix, C. B. et al. (2022). A comprehensive review of thermogravimetric analysis in lignocellulosic and algal biomass gasification. *Chem. Eng. J.*, 445, 136730. https://doi.org/10.1016/j.cej.2022.136730
50. Chen, D. et al. (2022). Insight into biomass pyrolysis mechanism based on cellulose, hemicellulose, and lignin: Evolution of volatiles and kinetics, elucidation of reaction pathways, and characterization of gas, biochar and bio-oil. *Combust. Flame*, 242. https://doi.org/10.1016/j.combustflame.2022.112142
51. Collard F. X. & Blin, J. (2014). A review on pyrolysis of biomass constituents: Mechanisms and composition of the products obtained from the conversion of cellulose, hemicelluloses and lignin. *Renew. Sustain. Energy Rev*., 38, 594–608. https://doi.org/10.1016/j.rser.2014.06.013
52. Werner, K. et al. (2014). Thermal decomposition of hemicelluloses. *J. Anal. Appl. Pyrolysis*, 110(1), 130–137. https://doi.org/10.1016/j.jaap.2014.08.013
53. Chen, L. et al. (2015). Study on pyrolysis behaviors of non-woody lignins with TG-FTIR and Py-GC/MS. *J. Anal. Appl. Pyrolysis*, 113, 499–507. https://doi.org/10.1016/j.jaap.2015.03.018
54. Onokwai, A. et al. (2022). Characterization of lignocellulose biomass based on proximate, ultimate, structural composition, and thermal analysis. *Mater. Today Proc*., 65(3), 2156–2162. https://doi.org/10.1016/j.matpr.2022.05.313
55. Guo, D. et al. (2021). Preparation and characteristic of high surface area lignin-based porous carbon by potassium tartrate activation. *Microporous Mesoporous Mater*., 326, 111340. https://doi.org/10.1016/j.micromeso.2021.111340.
56. Rim Choe, C. & Hee Lee K. (1992). Effect of processing parameters on the mechanical properties of carbonized phenolic resin. *Carbon*, 30(2), 247–249. https://doi.org/10.1016/0008-6223(92)90086-C
57. Kupgan, G., Liyana-Arachchi, T. P., & Colina, C. M. (2017). NLDFT pore size distribution in amorphous microporous materials. *Langmuir*, 33(42), 11138–11145. https://doi.org/10.1021/acs.langmuir.7b01961
58. Lee, S., Kim, J., Kim, W., & Roh, J. (2022). The effect of the heating rate during carbonization on the porosity, strength, and electrical resistivity of graphite blocks using phenolic resin as a binder. *Materials*, 15(9), 1–11. https://doi.org/10.3390/ma15093259